Supporting Information

Topological Self-Template Directed Synthesis of Multi-Shelled Intermetallic Ni_3Ga Hollow Microspheres toward Selective Hydrogenation of Alkyne

Mingzhen Hu+, Wenjuan Yang+, Shoujie Liu+, Wei Zhu, Yang Li, Zheng Chen, Rongan Shen, Weng-Chon Cheong, Yu Wang, Kebin Zhou,* Qing Peng, Chen Chen,* and Yadong Li

Experimental Section

Materials. All chemicals used were of analytical grade and used as received without further purification. Nickel(II) nitrate hexahydrate and urea were purchased from Tianjin Jinke Fine Chemical Institute. GalliuM(III) nitrate hydrate and stannous sulfate were purchased from Sigma-Aldrich. Glucose was purchased from J & K Scientific Ltd. The water used in all experiments was purified through a Millipore system.

Preparation of Ni_3Ga-MIHMs. In a typical synthesis of Ni_3Ga-MIHMs, 0.675 mmol of Nickel(II) nitrate hexahydrate and 0.225 mmol of GalliuM(III) nitrate hydrate were dissolved together in 65 mL of water. After stirring for half an hour, 10 mmol urea was then added under mild stirring to obtain a homogeneous solution. 0.03 mmol of glucose was further put into the above system and stirred until to obtain a clear solution. The whole solution was transferred into a Teflon lined stainless steel autoclave, sealed and maintained at 150 °C for 17 h. After cooling to room temperature, the resulted precipitates were isolated by centrifugation, washed with pure water for several times. At last, the product was dried in air at 60 °C overnight. The obtained solid sample was allowed for calcination at 600 °C in a tube furnace. The Ni_3Ga-MIHMs products were finally obtained by reducing the above calcinated intermediates by hydrogen at 630 °C.

Preparation of Ni-MHMs. In a typical synthesis of Ni-MHMs, 0.9 mmol of Nickel(II) nitrate hexahydrate were dissolved together in 65 mL of water. After stirring for half an hour, 10 mmol urea was then added under mild stirring to obtain a homogeneous solution. 0.03 mmol of glucose was further put into the above system and stirred until to obtain a clear solution. The whole solution was transferred into a Teflon lined stainless steel autoclave, sealed and maintained at 150 °C for 17 h. After cooling to room temperature, the resulted precipitates were isolated by centrifugation, washed with pure water for several times. At last, the product was dried in air at 60 °C overnight. The obtained solid sample was allowed for calcination at 600 °C in a tube furnace. The Ni_3Ga-MIHMs products were finally obtained by reducing the above calcinated intermediates by hydrogen at 550 °C.

Preparation of Ni_3Sn_4-MIHMs. In a typical synthesis of Ni_3Sn_4-MIHMs, 0.386 mmol of Nickel(II) nitrate hexahydrate and 0.514 mmol of stannous sulfate were dissolved together in 65 mL of water. After stirring for half an hour, 10 mmol urea was then added under mild stirring to obtain a homogeneous solution. 0.03 mmol of glucose was further put into the above system and stirred until to obtain a clear solution. The whole solution was transferred into a Teflon lined stainless steel autoclave, sealed and maintained at 160 °C for 17 h. After cooling to room temperature, the resulted precipitates were isolated by centrifugation, washed with pure water for several times. At last, the product was dried in air at 60 °C overnight. The obtained solid sample was allowed for calcination at 600 °C in a tube furnace. The Ni_3Sn_4-MIHMs products were finally obtained by reducing the above calcinated intermediates by hydrogen at 630 °C in a tube furnace.

Characterizations: The crystallographic structure of the obtained product was analyzed by powder X-ray diffraction (XRD, Bruker D8 Focus X-ray diffractometer, Cu Kα radiation, λ= 0.1542 nm). Transmission electron microscopy (TEM) analysis was carried out on JEM-2100F FETEM. The high angle annular dark field scanning TEM (HAADF-STEM) was operated at 200 kV equipped. X-ray photoelectron spectroscopy (XPS) analysis was conducted on ESCALAB 250 Xi X-ray photoelectron spectrometer with Al Kα radiation. The specific surface area measurement was conducted on a QuadraSorb SI automated surface area and pore size analyzer (Quantachrome Instruments). The element content of each sample was determined by inductively coupled plasma atomic emission spectroscopy (ICP-OES, Thermo Scientific).

XAFS measurements and analysis details: The X-ray absorption spectra at the Ni K-edge were recorded at 1W1B station in Beijing Synchrotron Radiation Facility (BSRF). The electron storage ring was operated at 2.5 GeV with a maximum current of 250 mA. Using Si(311) double-crystal monochromator, the data collection was carried out in transmission mode for Ni K-edge XAFS. All spectra were collected in ambient conditions. By using the third ionization chamber, standard compounds, Ni foil was measured simultaneously with the sample for energy calibration purposes. The acquired EXAFS data were processed according to the standard procedures using the ATHENA module implemented in the IFEFFIT software packages. The k^2-weighted EXAFS spectra were obtained by subtracting the post-edge background from the overall absorption and then normalizing with respect to the edge-jump step. Subsequently, k^2-weighted $\chi(k)$ data of Ni K-edge were Fourier transformed to real (R) space using a hanning windows (dk=1.0 $Å^{-1}$) to separate the EXAFS contributions from different coordination shells. To obtain the quantitative structural parameters around central atoms, least-squares curve parameter fitting was performed using the ARTEMIS module of IFEFFIT software packages.

Catalyst performance measurements: The catalytic properties of the prepared catalysts for selective hydrogenation of acetylene were evaluated under atmospheric pressure in a continuous flow fixed-bed quartz tubular reactor. In a typical process, 50 mg catalysts (based on Ni content) were mixed with quartz sand and placed in the reactor. The reactant gas mixture (0.65 vol % acetylene, 5 vol % hydrogen, 50.0 vol % ethylene balanced with argon) flowed through the reactor at a space velocity (SV) of 48000 mL/(g h). The composition of the outlet gas was recorded by gas chromatography. Conversion and selectivity were calculated according to previous report.[1]

Theoretical results: Calculations were performed using spin-polarized Kohn-Sham density functional theory (DFT). We used the generalized gradient approximation with the Perdew-Burke-Ernzerhof[2] exchange-correlation functional as implemented in the Vienna *ab initio* simulation package (VASP).[3,4] The valence orbitals of Ga (4s2, 4p1), Ni (3d, 4p), C (2s, 2p), and H (1s) were described by plane-wave basis sets with cutoff energies of 400 eV. The Gaussian smearing method with a width of 0.20 eV was used. According to the thermodynamics , a unit cell of 1:1 intermetallic cubic Ni_3Ga with a space group of Pm3m was used to model the catalyst structure. Bulk optimization yielded lattice parameters of a = c= b= 3.583 Å, which were in good agreement with the previous results.[5] The periodic slab model of Ni_3Ga (111) was employed to simulate the acetylene hydrogenation reactivity of intermetallic Ni_3Ga model based on thermodynamics. The Ni_3Ga (111) surface was modeled by $p(2 \times 2)$ four-atomic-layer supercells with the bottom two layers fixed, and the vacuum gap was set as 15 Å to avoid the interaction between the periodic images. All of the atoms in the Ni_3Ga were relaxed during the calculation. The Brillouin zone was sampled at (3× 3 × 1) and the Γ-point for the calculations of Ni_3Ga (111) surface and Ni (111) surface (the Ni (111) model is also chosen by thermodynamics), respectively. The convergence criteria for the energy and force were set to 10^{-4} eV and 0.05 eV/Å. For evaluating the energy barriers, all transition states and pathways were computed using the climbing image nudged elastic band (CI-NEB) method.[6,7]

The adsorption energies were calculated according to the equation, $E_{\mathrm{ads}} = E(\mathrm{adsorbate/substrate}) - [E(\mathrm{substrate}) + E(\mathrm{adsorbate})]$, where E(adsorbate/substrate), E(adsorbate) and E(substrate) are energies of the substrate with the adsorbate, the gas-phase molecule and the clean substrate, respectively. The reaction energy and barrier were calculated by $E_{\mathrm{r}} = E(\mathrm{FS}) - E(\mathrm{IS})$ and $E_{\mathrm{a}} = E(\mathrm{TS}) - E(\mathrm{IS})$, where E(IS), E(FS) and E(TS) are the energies of the corresponding initial state (IS), final state (FS), and transition state (TS), respectively. $\Delta E_a = E_{\mathrm{a}} - E_{\mathrm{des}}$ has been employed as a selectivity descriptor by the reported findings to investigate the selectivity of acetylene to ethylene.[8] To be noted, E_{a} is the hydrogenation barrier of C_2H_4 and E_{des} is the desorption energy of C_2H_4.

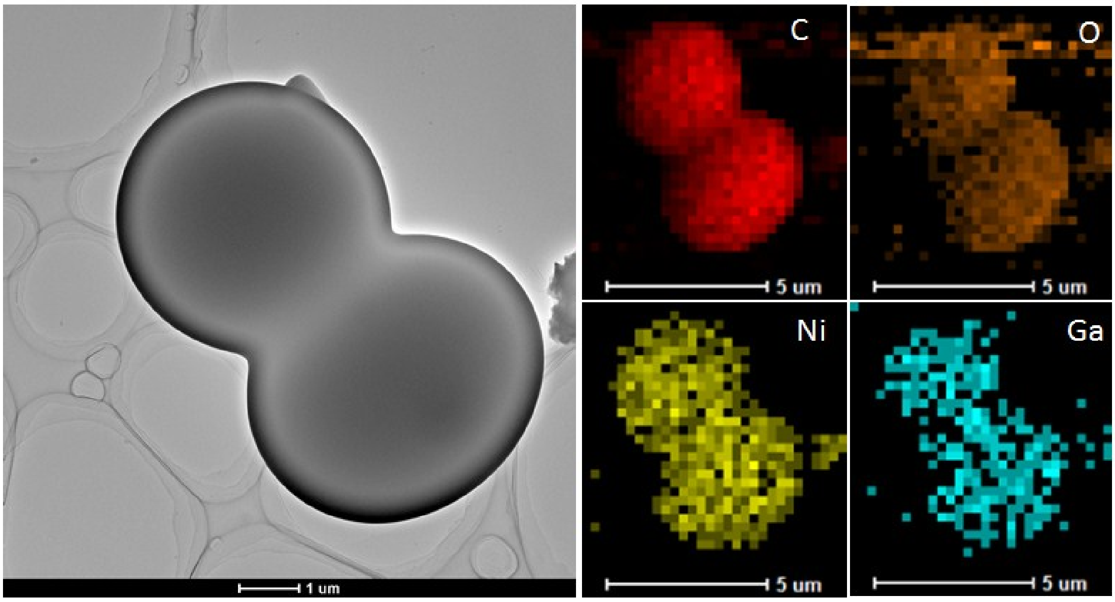

Figure S1. TEM image and corresponding EDS elementary mapping images of the composite solid spheres obtained by the hydrothermal treatment.

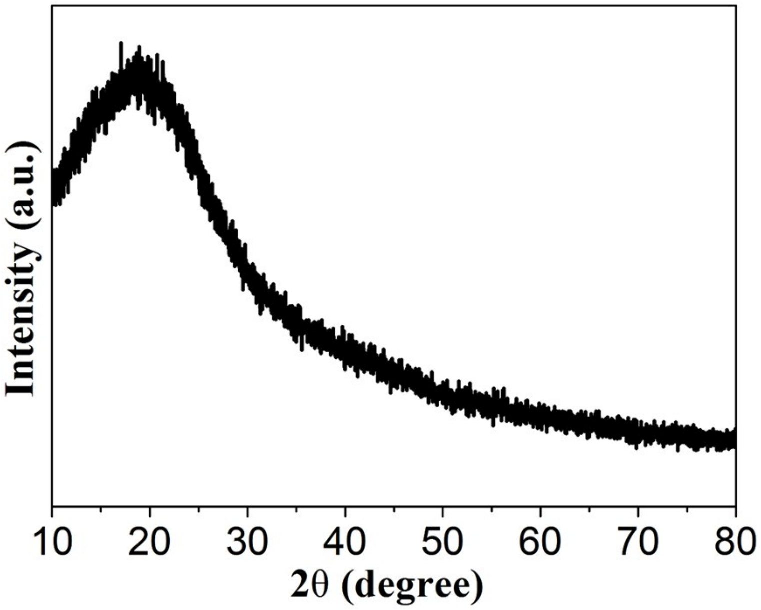

Figure S2. XRD pattern of the composite solid spheres obtained by the hydrothermal treatment.

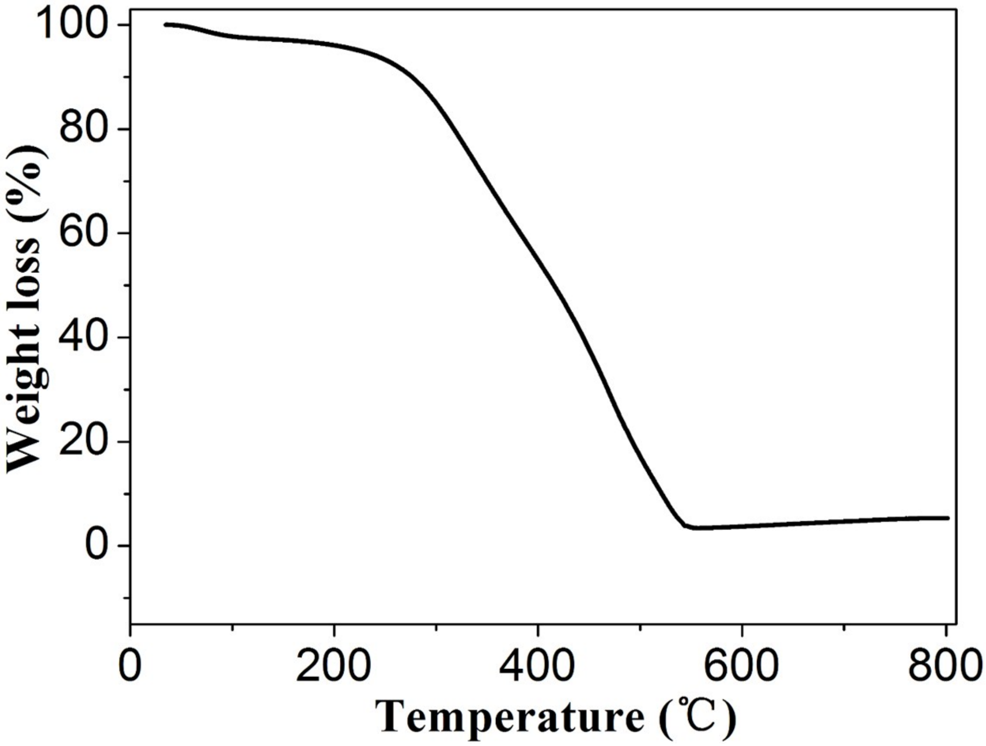

Figure S3. Thermogravimetric analysis profiles of the composite solid spheres obtained by the hydrothermal treatment.

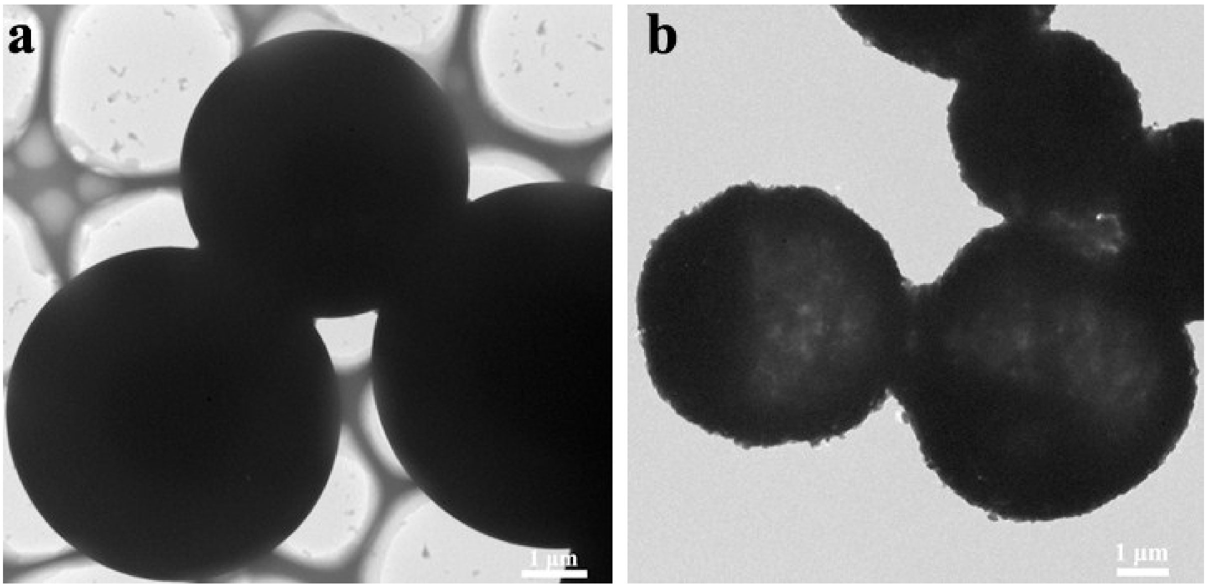

Figure S4. TEM image of the composite spheres (a) before and (b) after calcination treatment at 600 °C.

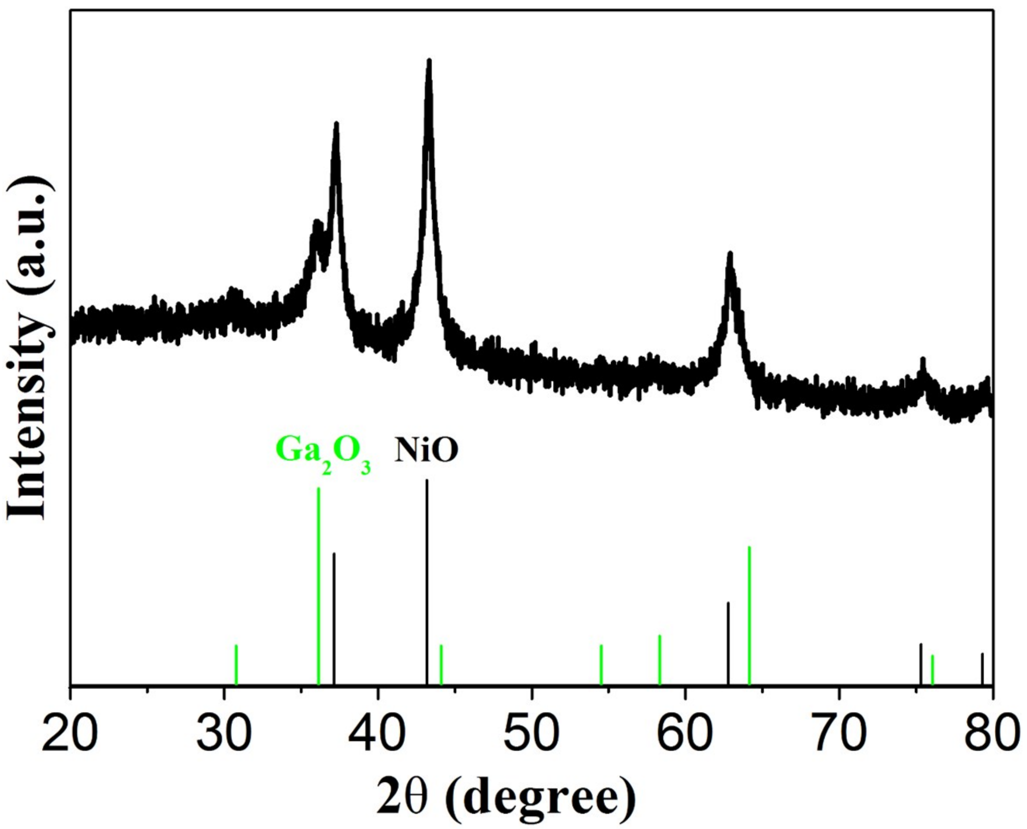

Figure S5. XRD pattern of the composite spheres after calcination at 600 °C.

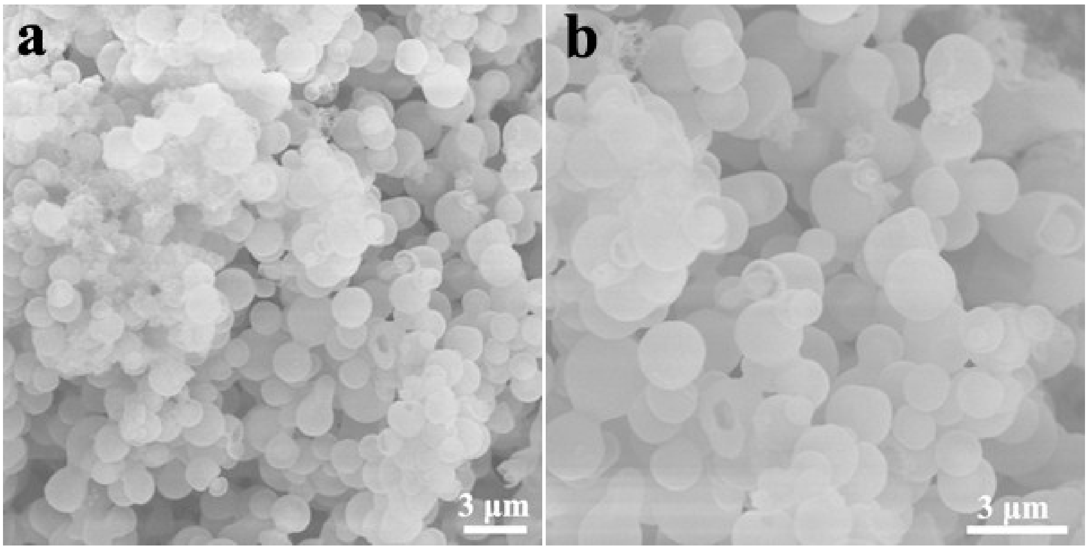

Figure S6. (a) and (b) SEM images of the prepared multi-shelled intermetallic Ni_3Ga hollow microsphere (Ni_3Ga-MIHM).

Table S1. Ni K-edge EXAFS curves fitting parameters.

Sample	Shell	N	R_j(Å)	σ^2 ($\times10^{-3}$Å^2)	E_0 (eV)
Ni_3Ga	Ni-Ni	4.0	2.6	4.7	4.3
	Ni-Ga	7.9	2.5	4.5	4.3

N, coordination number; R, distance between absorber and backscatter atoms; σ^2, Debye–Waller factor to account for both thermal and structural disorders;
ΔE_0, inner potential correction; R factor (%) indicates the goodness of the fit. Error bounds (accuracies) that characterize the structural parameters obtained by EXAFS spectroscopy were estimated as $N \pm 20\%$; $R \pm 1\%$; $\sigma^2 \pm 20\%$; $\Delta E_0 \pm 20\%$. S_0^2 was fixed to 0.97 as determined from Ni foil fitting.

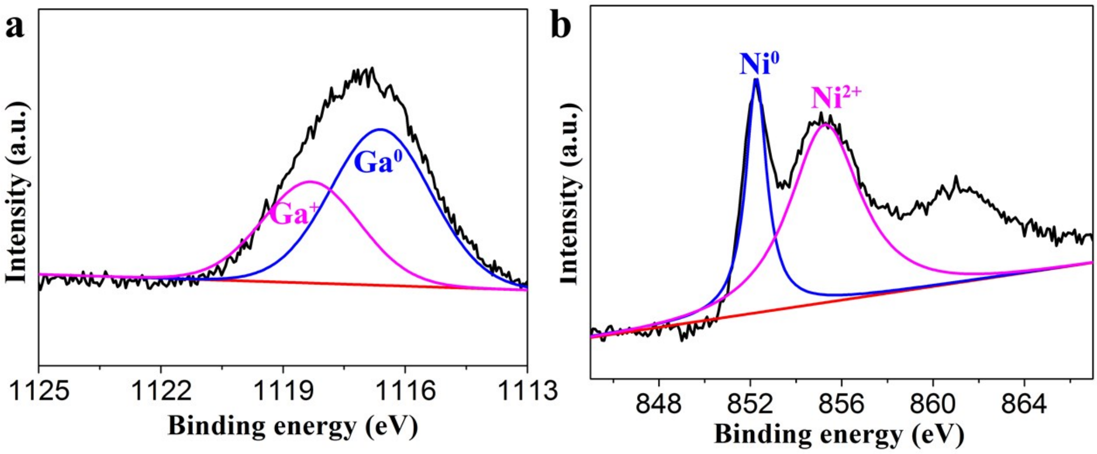

Figure S7. (a) Ga 2p XPS spectra of the prepared Ni_3Ga-MIHMs, (b) Ni 2p XPS spectra of the prepared Ni_3Ga-MIHMs.

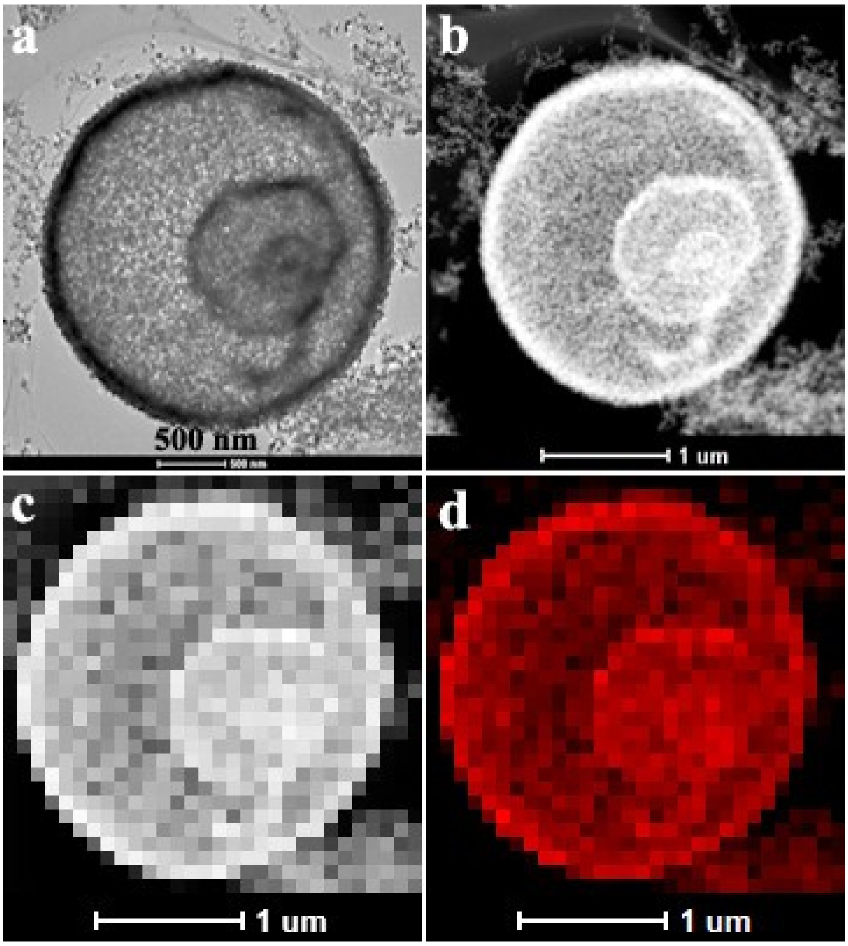

Figure S8. (a) TEM image, (b) and (c) HAADF-STEM images, (d) corresponding EDS elementary mapping image of the prepared multi-shelled Ni hollow microsphere (Ni-MHM).

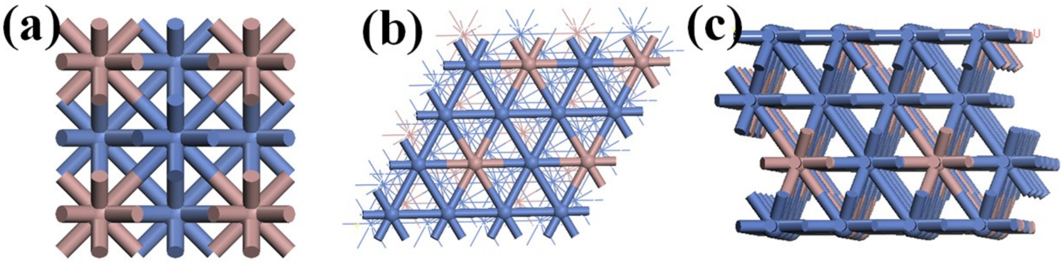

Figure S9. Structures of (a)Ni_3Ga; (b) top view of Ni_3Ga (111) surface and (c) side view of Ni_3Ga (111) surface (Ni: blue, Ga: pink).

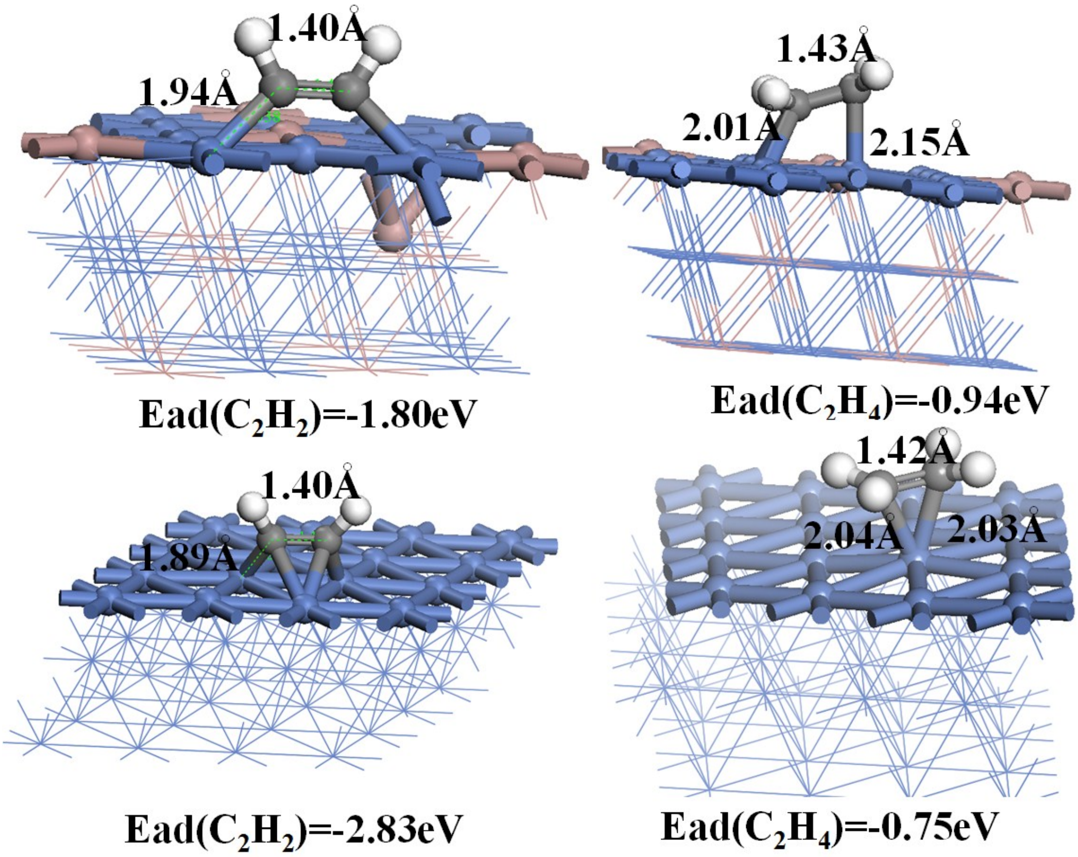

Figure S10. Adsorption configurations and energies of C_2H_2 and C_2H_4 on Ni_3Ga and Ni, respectively. (Ni: blue, Ga:pink, C: black, H: white).

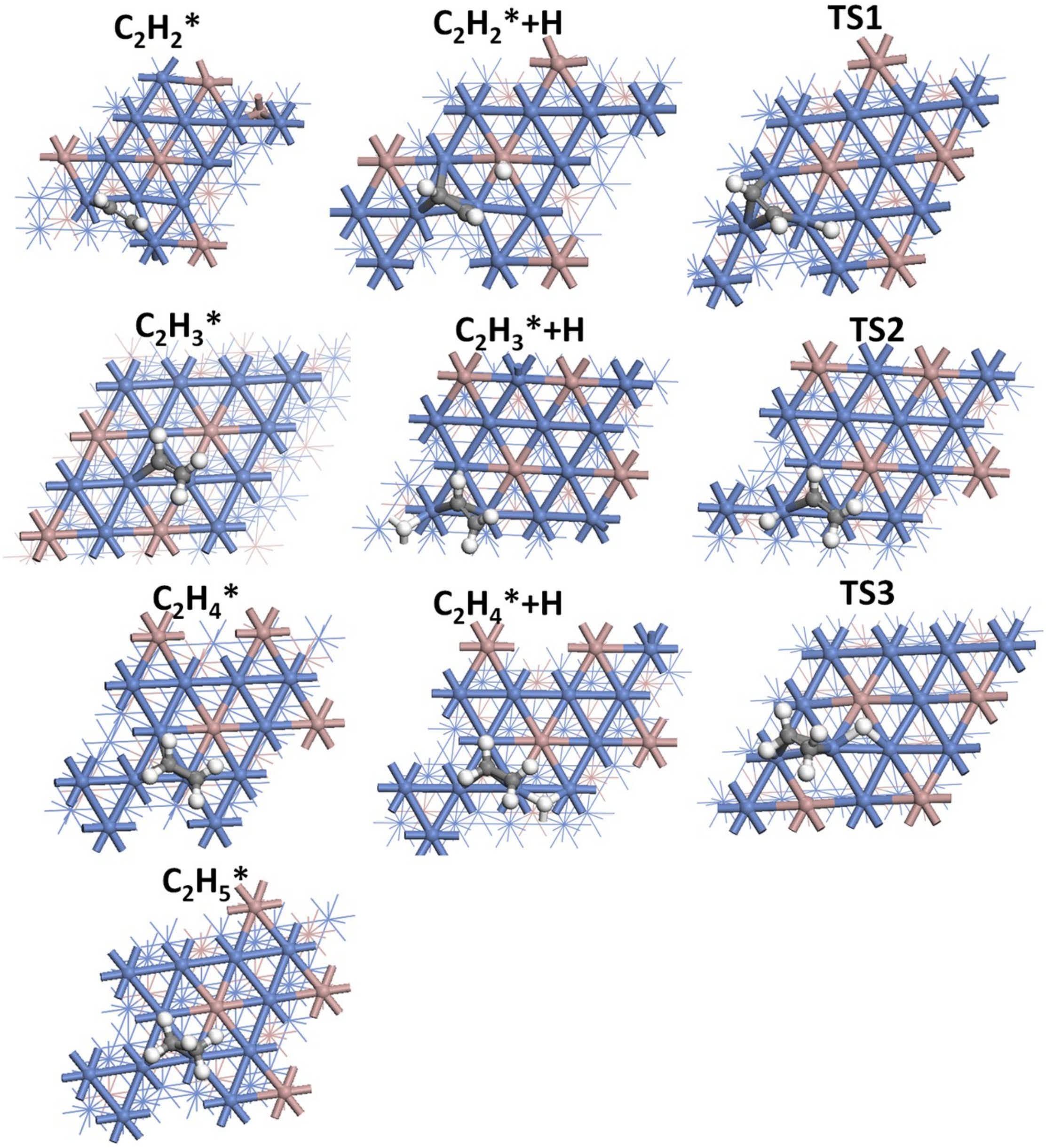

Figure S11. Structures of key stationary intermediates and transition states of C_2H_2 hydrogenation on Ni_3Ga. (Ni: blue, Ga: pink, C: black, H: white).

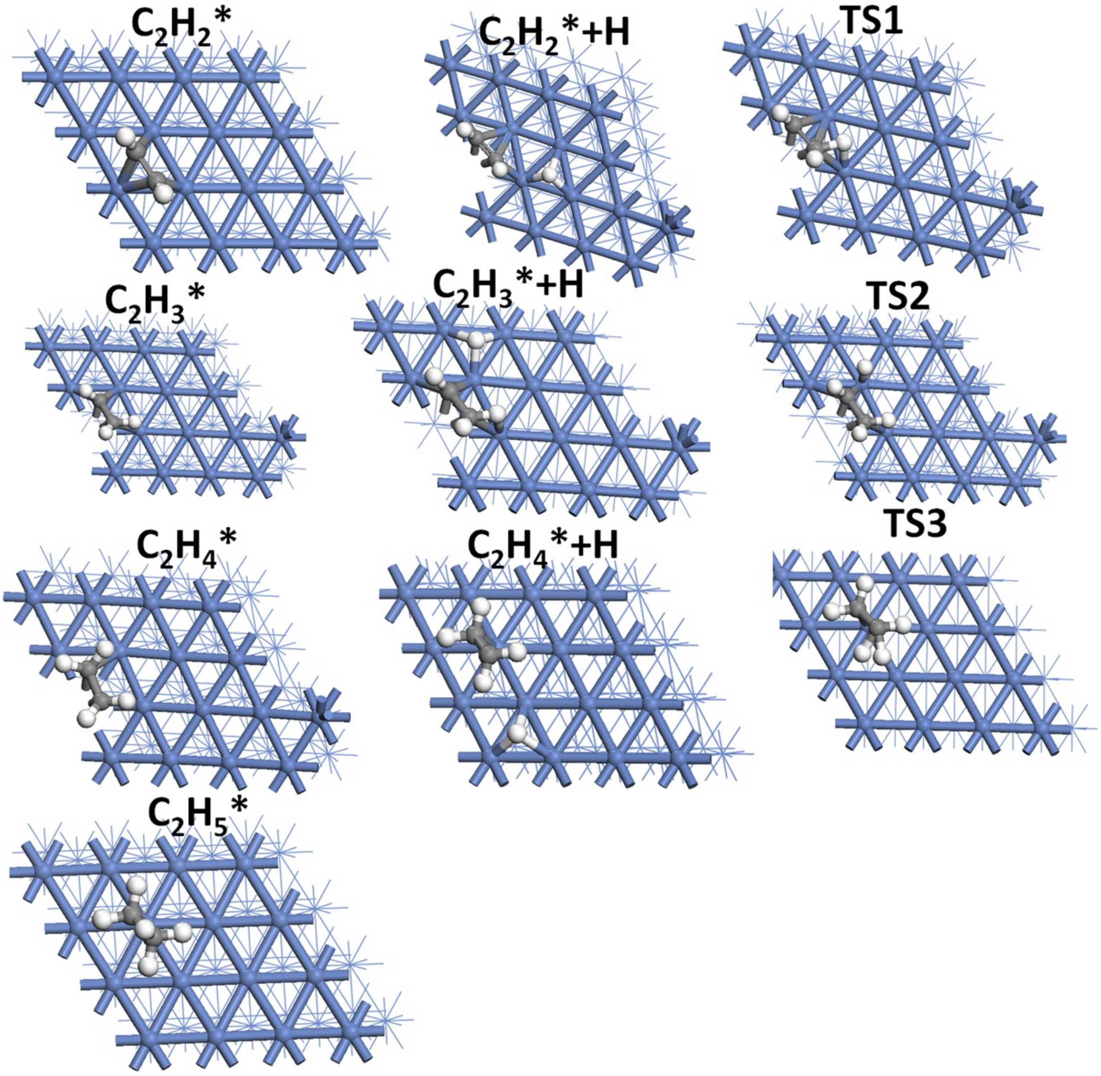

Figure S12. Structures of key stationary intermediates and transition states of C_2H_2 hydrogenation on Ni. (Ni: blue, C: black, H: white).

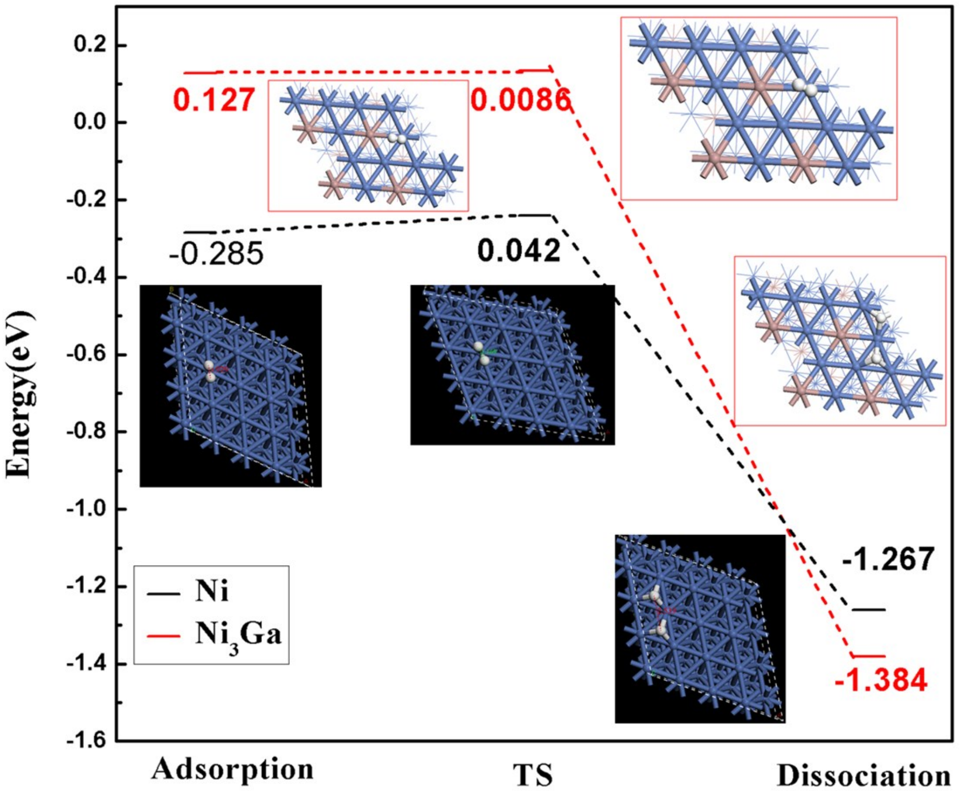

Figure S13. Potential energy diagrams of H_2 dissociation on Ni_3Ga and Ni, respectively. Numbers in the parentheses indicate the barriers of elementary steps. (Ni: blue, Ga: pink, C: black, H: white).

Table S2. Barrier (E_a, eV) and reaction energy (E_r, eV) for acetylene on the Ni_3Ga

	E_a (eV)	E_r (eV)
C_2H_2+H→C_2H_3 (TS1)	1.08	-0.509
C_2H_3+H→C_2H_4 (TS2)	0.61	-0.027
C_2H_4+H→C_2H_5 (TS3)	1.22	0.04

Table S3. Barrier (E_a, eV) and reaction energy (E_r, eV) for acetylene on Ni.

	E_a (eV)	E_r (eV)
C_2H_2+H→C_2H_3 (TS1)	0.92	-1.95
C_2H_3+H→C_2H_4 (TS2)	0.68	0.17
C_2H_4+H→C_2H_5 (TS3)	0.39	-0.23

Table S4. Crystal formation energies (eV) of Ni_3Ga and Ni_3Sn_4. The crystal formation energy is defined as the energy (per unit cell) required to form the crystals relative to pure metal.

Intermetallic phase	Ni_3Ga	Ni_3Sn_4
Formation energy (eV)	-16.35	-59.46

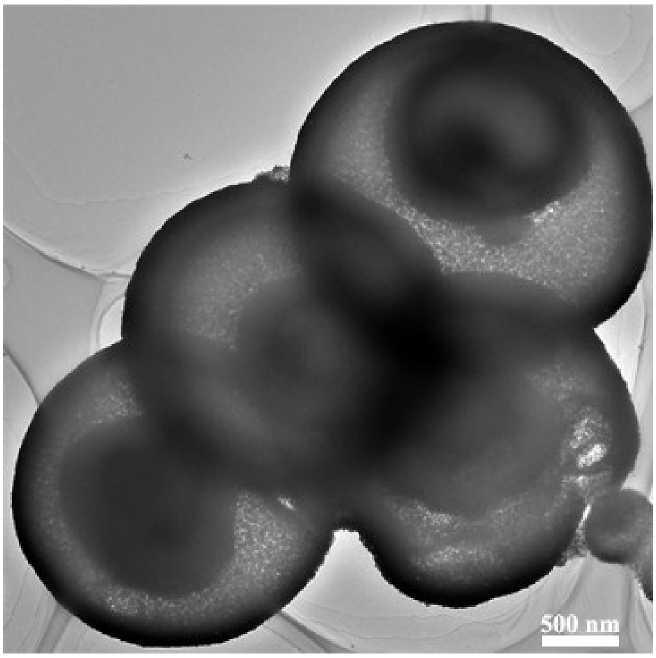

Figure S14. TEM image of the prepared Ni_3Sn_4-MIHMs.

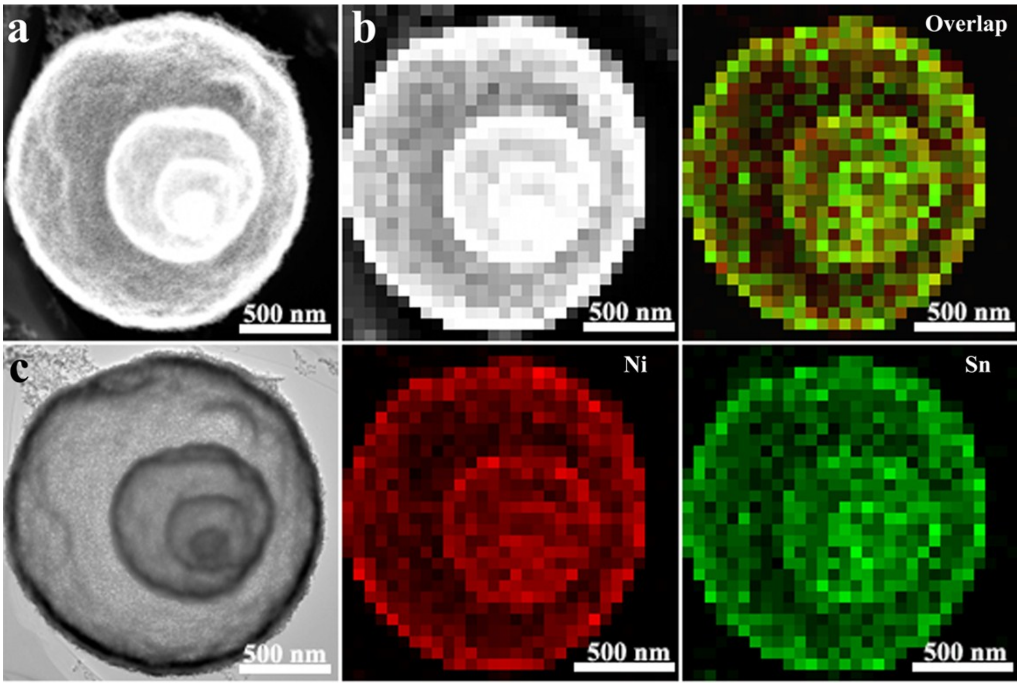

Figure S15. (a) HAADF-STEM of Ni_3Sn_4-MIHMs. (b) HAADF-STEM and EDS elementary mapping images of the Ni_3Sn_4-MIHMs. (c) TEM image of Ni_3Sn_4-MIHMs.

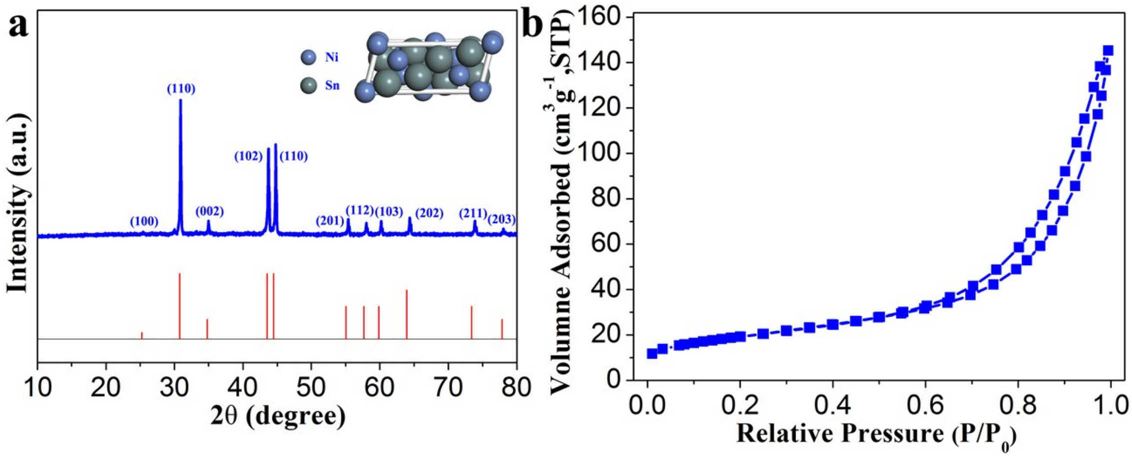

Figure S16. (a) XRD pattern and (b) Nitrogen adsorption-desorption isotherm of the prepared Ni_3Sn_4-MIHMs.

References

(1) Yang, J.; Zhang, F.; Lu, H.; Hong, X.; Jiang, H.; Wu, Y.; Li, Y. *Angew. Chem. Int. Ed.* **2015**, *54*, 10889.

(2) Perdew, J. P.; Burke, K.; Ernzerhof, M. *Phys. Rev. Lett.* **1996**, *77*, 3865.

(3) Kresse, G.; Furthmüller, J. *Physical Review B* **1996**, *54*, 11169.

(4) Kresse, G.; Furthmüller, J. *Computational Materials Science* **1996**, *6*, 15.

(5) Nozawa, K.; Endo, N.; Kameoka, S.; Pang Tsai, A.; Ishii, Y. *J. Phys. Soc. Jpn.* **2011**, *80*, 064801.

(6) Henkelman, G.; Uberuaga, B. P.; Jónsson, H. *The Journal of Chemical Physics* **2000**, *113*, 9901.

(7) Henkelman, G.; Jónsson, H. *The Journal of Chemical Physics* **2000**, *113*, 9978.

(8) Yang, B.; Burch, R.; Hardacre, C.; Headdock, G.; Hu, P. *ACS Catal.* **2012**, *2*, 1027.